JCI insight

Tuft cells are required for a rhinovirus-induced asthma phenotype in immature mice

Yiran Li, … , Ichiro Matsumoto, Marc B. Hershenson

JCI Insight. 2023. https://doi.org/10.1172/jci.insight.166136.

Research In-Press Preview **Pulmonology**

Infection of immature mice with rhinovirus (RV) induces an asthma-like phenotype consisting of type 2 inflammation, mucous metaplasia, eosinophilic inflammation and airways hyperresponsiveness which is dependent on IL-25 and type 2 innate lymphoid cells (ILC2s). Doublecortin-like kinase (DCLK)-1$^+$ tuft cells are a major source of IL-25. We sought to determine the requirement of tuft cells for the RV-induced asthma phenotype in wild-type mice and mice deficient in Pou2f3, a transcription factor required for tuft cell development. C57Bl/6 mice infected with RV-A1B on day 6 of life and RV-A2 on day 13 of life showed increased DCLK1$^+$ positive tuft cells in the large airways. Compared to wild-type mice, RV-infected *Pou2f3*$^{-/-}$ mice showed reductions in IL-25 mRNA and protein expression, ILC2 expansion, type 2 cytokine expression, mucous metaplasia, lung eosinophils and airway methacholine responsiveness. We conclude that airway tuft cells are required for the asthma phenotype observed in immature mice undergoing repeated RV infections. Furthermore, RV-induced tuft cell development provides a mechanism by which early life viral infections could potentiate type 2 inflammatory responses to future infections.

Tuft cells are required for a rhinovirus-induced asthma phenotype in immature mice

Yiran Li[1*], Mingyuan Han[1*], Shilpi Singh[1], Haley A. Breckenridge[1], , Jordan E. Kreger[1], Claudia C. Stroupe[1], Daniel A. Sawicky[1], Shiuhyang Kuo[1], Adam M. Goldsmith[1], Fang Ke[2], Anukul T. Shenoy[2,3], J. Kelley Bentley[1], Ichiro Matsumoto[4] and Marc B. Hershenson[1,5]

*These two authors share the first author position. YL helped design the research, performed experiments, analyzed data, interpreted results of the experiments, prepared figures, drafted the manuscript, and approved the final version of the manuscript. M.H. helped design the research, performed experiments, analyzed data, interpreted results of experiments, prepared figures, and drafted the manuscript, and approved the final version of the manuscript.

[1]Department of Pediatrics, University of Michigan Medical School; [2]Department of Microbiology and Immunology, University of Michigan Medical School; [3]Department of Internal Medicine, University of Michigan Medical School; [4]Monell Chemical Senses Center, Philadelphia; [5]Department of Molecular and Integrative Physiology, University of Michigan Medical School.

Corresponding author: Marc B. Hershenson, M.D., 1150 W. Medical Center Drive, Ann Arbor, MI 48109-5688; phone, 734-936-4200; E mail: mhershen@umich.edu

Conflict of interest statement: The authors have declared that no conflict of interest exists.

Abstract

Infection of immature mice with rhinovirus (RV) induces an asthma-like phenotype consisting of type 2 inflammation, mucous metaplasia, eosinophilic inflammation and airways hyperresponsiveness which is dependent on IL-25 and type 2 innate lymphoid cells (ILC2s). Doublecortin-like kinase (DCLK)-1+ tuft cells are a major source of IL-25. We sought to determine the requirement of tuft cells for the RV-induced asthma phenotype in wild-type mice and mice deficient in Pou2f3, a transcription factor required for tuft cell development. C57Bl/6 mice infected with RV-A1B on day 6 of life and RV-A2 on day 13 of life showed increased DCLK1+ positive tuft cells in the large airways. Compared to wild-type mice, RV-infected *Pou2f3*$^{-/-}$ mice showed reductions in IL-25 mRNA and protein expression, ILC2 expansion, type 2 cytokine expression, mucous metaplasia, lung eosinophils and airway methacholine responsiveness. We conclude that airway tuft cells are required for the asthma phenotype observed in immature mice undergoing repeated RV infections. Furthermore, RV-induced tuft cell development provides a mechanism by which early life viral infections could potentiate type 2 inflammatory responses to future infections.

Introduction

Tuft cells of the respiratory and gastrointestinal tract are characterized by the presence of a tuft of blunt, squat microvilli (~120-140/cell) on the cell surface (1). Tuft cells are chemosensory cells that express elements of the taste transduction system including bitter taste receptors (T2Rs), sweet and umami taste receptors (T1Rs), Gnat3 (also known as α-gustducin) and transient receptor potential cation channel subfamily M member (TRPM)-5 (2), a calcium-activated non-selective cation channel. Tuft cells also express doublecortin-like kinase 1 (DCLK1) (3), a serine/threonine protein kinase involved in several different cellular processes, including binding of microtubules and regulation of microtubule polymerization, neuronal migration, retrograde transport, neuronal apoptosis and neurogenesis. It has been demonstrated that Pou2f3, a POU homeodomain transcription factor, is expressed in TRPM5-expressing chemosensory cells and is necessary for their generation (4-6).

Tuft cells in the sinonasal and lung epithelia displaying taste cell-like molecular features are also termed solitary chemosensory cells, or SCCs (7). Stimulation of T2Rs in SCCs has been shown to regulate respiratory rate (2, 7), acetylcholine release (8) and a calcium wave that propagates through gap junctions to the surrounding respiratory epithelial cells, stimulating secretion of antimicrobial peptides (9). DCLK1+ TRPM5+ SCCs develop in the distal lung after severe influenza injury (10-12).

Tuft cells of the respiratory and gastrointestinal tract have also been implicated in type 2 immune responses. Gastrointestinal DCLK1+ tuft cells constitutively express IL-25, and expression was further increased after helminth infection, leading to IL-13 secretion by type 2 innate lymphoid cells (ILC2s) (13-15). The innate cytokines IL-25, IL-33 and thymic stromal lymphopoietin (TSLP) have additive effects on ILC2 function and augmenting cellular

responsiveness to each other via upregulation of their cellular receptors (16, 17). In the airways, single-cell RNA-sequencing has demonstrated IL-25 expression in mouse tracheal tuft cells (18, 19), and IL-25 reporter mice show that tracheal tuft cells are a primary source of IL-25 (13, 20). Aeroallergens induce DCLK1+ IL-25+ tracheal tuft cell expansion in mice (20, 21) and DCLK1+ tuft cells produce IL-25 in patients with chronic rhinosinusitis with nasal polyps (22).

We have shown that rhinovirus (RV)-A1B infection of 6 day-old mice, but not mature mice, induces mucous metaplasia and airway hyperresponsiveness (23) which is associated with ILC2 expansion and dependent on IL-13, IL-25, IL-33 and TSLP (17, 24). ILC2s are required and sufficient for the asthma-like phenotype (25). Finally, we observed that RV-A1B infection on day 6 of life augmented the impact of a second RV infection administered one week later, amplifying type 2 cytokine expression, mucus production and airways resistance in an ILC2-dependent manner (26). Since DCLK1+ tuft cells are a major source of IL-25 in the gut (13-15), we examined the contribution of these cells to the RV-induced asthma-like phenotype in immature mice.

Results

Early-life RV infection expands the number of DCLK1+ airway tuft cells. To determine if early life RV infection induces airway tuft cell expansion, wild-type C57Bl/6J mice were inoculated with sham HeLa cell lysate or RV-A1B on day six of life and inoculated with sham or a heterologous RV serotype, RV-A2, on day 13 of life (26). Seven days after inoculation with sham or RV-A2 (day 20 of life), lungs were for stained with a monoclonal antibody against DCLK1, a marker of murine tuft cells (3). Lungs from sham-infected mice showed an absence of DCLK1+ cells. The number and percentage of airway DCLK1+ cells significantly increased in mice with RV-A1B on day six of life (Figure 1A and 1B). DCLK1+ cells were found in intrapulmonary large airways with psuedostratifed or cuboidal epithelium. There was no change in the number of tuft cells following RV-A2 infection on day 13 of life. However, infection of mice with RV-A2 one week after the previous RV-A1B infection further increased the number and percentage of airway DCLK1+ cells compared to RV-A1B alone (Figure 1A and 1B). Finally, RV infected- *Pou2f3*$^{-/-}$ mice showed an absence of DCLK+ cells as expected (Figure 1C).

To confirm the identity of DCLK1+ tuft cells, we infected immature ChAT-eGFP mice with RV-A1B and RV-A2. Choline acetyltransferase expression is part of a transcriptional signature shared by all murine tuft cells (27). We found colocalization of DCLK1 and eGFP, confirming that DLCK1+ cells were indeed tuft cells (Figure 2A). Also, compared to wild-type mice, lung mRNA expression of tuft cell markers *Dclk1* and *Alox5* was decreased in double-infected *Pou2f3*$^{-/-}$ mice (Figure 2B).

Krt5-positive distal airway stem cells are essential for lung regeneration after influenza infection (28). We found Krt5+ cells in the trachea and rarely in the cartilagenous airways of the

lung (Figure 2C). However we were only able to find one example of Krt5+ cells neighboring a DCLK1+ tuft cell (in the trachea). Finally, we measured RV copy number one day after secondary infection with sham or RV-A2 (Figure 2D). *Pou2f3*$^{-/-}$ mice showed no changes in viral copies compared to wild-type mice.

Pou2f3$^{-/-}$ *mice show reduced innate cytokine expression after heterologous RV infection.* Pou2f3, a POU homeodomain transcription factor, is required for tuft cell development (4-6). Mice with Pou2f3 deficiency show an absence of TRPM-5- and DCLK1- expressing brush cells in trachea and digestive tracts (6). We have shown that RV-A1B infection of six-day-old mice induces mucous metaplasia and airway hyperresponsiveness which is associated with ILC2 expansion and dependent on IL-13, IL-25, IL-33 and TSLP (17, 24). Since the tuft cell is a major cellular source of IL-25 in the gut (13-15) and trachea (13, 18-20), we employed mice with Pou2f3 deficiency to examine the role of airway tuft cells in the innate cytokine response to heterologous RV infections. Based on previous studies showing differential kinetics for IL-25, TSLP and IL-33 expression (17), lung mRNA and protein were harvested at day 20 of life (7 days after the last treatment) for IL-25 and TSLP and on day 14 (one day after the last treatment) for IL-33. Mice undergoing RV-A1B infection on day 6 of life and sham infection on day 13 showed significantly increased mRNA and protein expression of IL-25 on day 20 of life compared to sham-infected mice (Figure 3A). Heterologous infection with RV-A2 on day 13 of life further increased IL-25 expression. Compared to wild-type mice, double-infected *Pou2f3*$^{-/-}$ mice showed reduced mRNA and protein expression of IL-25 on day 20 of life, suggesting that tuft cells are required for the IL-25 response to heterologous RV infections. As previously shown (17), TSLP mRNA expression was not increased by viral infection. However, heterologous infection with two RV serotypes induced TSLP protein (Figure 3B). Compared to

wild-type mice, double-infected *Pou2f3*$^{-/-}$ mice showed reduced TSLP expression on day 20 of life, suggesting that tuft cells are also required for RV-induced TSLP protein production. However, the Pou2f3 deficiency did not attenuate IL-25 or TSLP expression in mice infected with a single RV infection. Finally, double infection with two RV serotypes significantly increased both IL-33 mRNA and protein expression. IL-33, which is not produced by tuft cells, was unaffected by the Pou2f3 deficiency (Figure 3C).

Pou2f3$^{-/-}$ *mice show reduced lung ILC2s.* In our model, IL-25, IL-33, and TSLP cooperate in RV-induced ILC2 expansion and mucous metaplasia, each having additive effects on ILC2 function and augmenting cellular responsiveness to each other via upregulation of their cellular receptors (17). We therefore examined the requirement of Pou2f3 for ILC2 expansion one week after heterologous RV infections. Consistent with our previous results (26), infection with RV-A1B and RV-A2 increased the number of lineage-negative, ST2+, CD127+ cells by flow cytometry (Figure 4A, 4B). ILC2 number was significantly reduced, though not abolished, in *Pou2f3*$^{-/-}$ mice following heterologous infection (Figure 4B).

Pou2f3$^{-/-}$ *mice show reduced type 2 inflammation after double RV infection.* To determine the downstream effects of airway tuft cell defciency, we measured cytokine mRNA expression in wild-type C57BL/6J and tuft cell-deficient *Pou2f3*$^{-/-}$ mice. Lungs were harvested for type 2 cytokine mRNA and protein on day 20 of life and harvested for pro-inflammatory cytokine mRNA and protein on day 14 of life. Contrasted to mice infected with a single RV serotype, heterologous infection with RV-A2 on day 13 of life induced exaggerated type 2 cytokine mRNA expression. Double-infected *Pou2f3*$^{-/-}$ mice showed significantly reduced mRNA expression of IL-4, IL-5 and IL-13 (Figure 5A), demonstrating that tuft cells are required for the type 2 cytokine response to heterologous RV infection.

In contrast to IL-4, IL-5, IL-13, mRNA expression of IL-1β and TNF-α, both considered type 1 cytokines, decreased after infection with RV-A2, suggesting that RV infection on day 6 of life skewed the response to subsequent heterologous RV infection towards a type 2 phenotype (Figure 5B). Double-infected *Pou2f3*$^{-/-}$ mice did not show a change in TNF-α or IL-1β mRNA cytokine expression. Unexpectedly, *Pou2f3*$^{-/-}$ mice infected with both serotypes showed increased mRNA expression of IFN-γ compared to mice infected with RV-A1B alone.

Effects of Pou2f3 deficiency on the asthma phenotype. Contrasted to a single infection with RV-A1B, heterologous RV infections increased the number of Periodic acid-Schiff (PAS)-positive cells (Figure 6A and 6B). A similar pattern was observed for the mRNA expression of Muc5ac and Gob5 (Figure 6C). Since PAS detects mucosubstances such as glycoproteins, glycolipids and mucins, together these data indicate heterologous viral infection induces mucous metaplasia. In contrast, *Pou2f3*$^{-/-}$ mice lacking tuft cells exhibited attenuated PAS staining. Next, we measured lung eosinophils by flow cytometry. Compared to wild-type RV-A1B and RV-A2-infected mice, double-infected *Pou2f3*$^{-/-}$ mice showed reduced lung eosinophils (Figure 7A, B). Finally, we measured changes in airways resistance in viral-infected mice after injection of methacholine into the retro-orbital venous sinus (Figure 7C). *Pou2f3*$^{-/-}$ mice showed a significantly lower response to methacholine than wild-type mice.

Discussion

Tuft cells of the lower airway epithelium are chemosensory cells that express TRPM-5, a calcium-activated cation channel of the bitter taste transduction system (2), and DCLK1, a serine/threonine protein kinase involved in the regulation of microtubule polymerization. In addition to a chemosensory function, tuft cells also play a role in inflammation. In mice, DCLK1+ chemosensory cells develop in the distal lung after severe influenza injury (10-12). Gastrointestinal DCLK1+ tuft cells constitutively express IL-25, and expression is further increased after helminth infection, leading to IL-13 secretion by ILC2s (13-15). In the respiratory system, *Alternaria* and house dust mite exposure induce DCLK1+ IL-25+ airway tuft cell expansion (20). Tracheal tuft cells are a primary source of IL-25 in mice (13, 18-20), and tuft cells produce IL-25 in human patients with chronic rhinosinusitis with nasal polyps (22).

Wheezing-associated respiratory infections with RV are associated with asthma development later in life (29-31). On average, children experience four acute respiratory infections the first year of life, the majority of which are RV (32). To determine if RV infection early in life could promote development of an asthma phenotype, we infected six-day-old mice with RV-A1B. We found that early-life RV infection increased lung ILC2s, mucous metaplasia and airways hyperresponsiveness (23, 24). We also observed that RV-A1B infection at day 6 of life augmented the impact of a second RV infection administered one week later, amplifying type 2 cytokine expression, mucus production and airways resistance in an ILC2-dependent manner (26). We found that epithelial-derived innate cytokines cooperate to promote the RV-induced phenotype, each having additive effects on ILC2 function and augmenting cellular responsiveness to each other via upregulation of their cellular receptors (17). We therefore investigated whether infection with RV in early life modulates tuft cell development. We found

that early-life RV infection induced the appearance of DCLK1+ tuft cells and that heterologous infection with both RV-A1B and RV-A2 caused a further increase in DCLK1+ cells. We also determined the requirement of tuft cells for the RV-induced asthma phenotype in wild-type mice and mice deficient in Pou2f3, a transcription factor required for tuft cell development. *Pou2f3*$^{-/-}$ mice undergoing heterologous RV infections showed significant reductions in IL-25 and TSLP protein expression, ILC2 expansion, type 2 cytokine expression mucous metaplasia, lung eosinophils and airways methacholine responsiveness. We conclude that airway tuft cells, by virtue of their production of IL-25, are required for the exaggerated asthma phenotype observed in immature mice undergoing repeated RV infections. As far as we aware, this is the first report demonstrating the requirement of tuft cells for a viral-induced asthma phenotype. Tuft cells have previously been shown to be required for allergic airways disease in *Alternaria*-exposed mice (21, 33).

We did not determine the mechanism by which viral infection increases tuft cell development. Epithelial damage itself could elicit a remodeling program characterized leading to tuft cell development. As noted above, DCLK1+ chemosensory cells develop in the distal lung after severe influenza injury (10, 11). After influenza infection, DCLK1+ TRPM5+ SCCs co-express p63 and arise near Krt5+ cells (10), suggesting a common origin with p63+ Krt5+ distal airway epithelial cells implicated in lung regeneration (34). However, after RV infection, DCLK1+ tuft cells were found primarily in the proximal intrapulmonary airways and were not associated with Krt5+ cells. This is consistent the minimal damage to the airway epithelium after RV infection (35). Other mechanisms promoting tuft cell development are possible: In the intestine, tuft cell hyperplasia following parasitic infection is dependent on IL-

13-producing ILC2s (13). Finally, aeroallergen-induced airway tuft cell expansion in adult mice is dependent on cysteinyl leukotrienes (20).

While Pou2f3 deficient mice lacking tuft cells showed an attenuated response to double RV infection, the limited response to a single infection on day 6 of life was generally maintained. Specifically, IL-25 and TSLP production in RV-A1B-induced Pou2f3 deficient mice was not decreased, suggesting that tuft cells are not the only cellular source of these cytokines in 6-day-old mice. Alveolar macrophages, eosinophils and other immune cells may also produce IL-25 (36, 37). Another possibility is that tuft cells do not require Pou2f3 during early postnatal development.

We would like to comment on the small number of tuft cells we found in the airways of immature mice infected with RV. Airways from uninfected mice showed no DCLK+ cells. After heterologous RV infection, the number of tuft cells constituted approximately 1% of the airway epithelium. The paucity of DCLK1+ cells is consistent with previous studies employing single cell RNASeq showing that tuft cells constitute a rare population of chemosensory cells in the airways (18). Previous studies have found few (<1%) (12) or no tuft cells (10, 33, 38) beyond the trachea in naïve mice. On the other hand, ~~However,~~ recent studies in influenza-infected (10) and allergen-challenged mice (21, 33), as well as human patients with chronic rhinosinusitis, show them to be more numerous (22). Factors influencing the number of tuft cells identified may include age, species, airway generation, intensity of the provoking stimulus, length of time after the provoking stimulus, and method of identification, for example single cell RNASeq vs immunostaining. Also, it is conceivable that we missed a subset of DCLK1-negative tuft cells (21).

We conclude that airway IL-25-producing tuft cells are required for the exaggerated asthma phenotype observed in immature mice undergoing repeated RV infections. Furthermore, viral infection increases airway tuft cell development, providing a potential mechanism by which early life viral infections could potentiate type 2 inflammatory responses to future infections, skewing the immune response towards an asthma phenotype.

Methods

Animals. C57BL/6J mice and B6.Cg-Tg(RP23-268L19-EGFP)2Mik/J (ChAT-eGFP mice) were purchased from Jackson Laboratory (Bar Harbor, ME). To elucidate the function of tuft cells in our model, we employed *Pou2f3*$^{-/-}$ mice, as described elsewhere (4). Mice were bred in house in pathogen-free facility within the Unit for Laboratory Animal Medicine at the University of Michigan.

Generation of RV-A1B and RV-A2. RV-A1B and RV-A2 (ATCC, Manassas, VA), minor group viruses that infect mouse cells (39), were partially purified from infected HeLa cell lysates by means of ultrafiltration with a 100-kDa cutoff filter and titered by using a plaque assay as described previously (40, 41). Intact virus does not go through the filter and is concentrated. Similarly concentrated and purified HeLa cell lysates were used for sham infection.

RV infections. Mice were inoculated with 15 µl of HeLa cell lysate, 1.5 x 10^6 plaque-forming units (PFU) of RV-A1B or 1.5 x 10^6 PFU of RV-A2 through the intranasal route under Forane anesthesia. Mice were treated as follows: 1) day 6 sham + day 13 sham; 2) day 6 RV-A1B + day 13 sham; 3) day 6 sham + day 13 RV-A2; and 4) day 6 RV-A1B + day 13 RV-A2.

Real-time quantitative PCR. Lung RNA was extracted with Trizol (Invitrogen~~, Carlsbad, CA~~) and isolated using an RNeasy kit (Qiagen, MD). cDNA was synthesized from 2 µg of RNA using high capacity cDNA synthases kit (Applied Biosystems) and subjected to quantitative real-time PCR using specific primers (Table) for mRNA. The level of gene expression for each sample was normalized to GAPDH. To quantify viral copy number, qPCR for positive-strand viral RNA was conducted using RV-specific primers and probes (forward primer: 5'-GTGAAGAGCCSCRTGTGCT-3'; reverse primer: 5'-GCTSCAGGGTTAAGGTTAGCC-3'; probe: 5'-FAM-TGAGTCCTCCGGCCCCTGAATG-TAMRA-3').

Histology and immunofluorescence. Lungs were fixed with 10% formaldehyde overnight and paraffin embedded. Blocks were sectioned at 500 μm intervals at a thickness of 5 μm, and each section was deparaffinized, hydrated and stained. To visualize mucus, sections were stained with periodic acid-Schiff (PAS; Sigma-Aldrich). PAS staining in the airway epithelium was quantified by NIH ImageJ software. Six separate mouse lungs of either wild-type or *Pou2f3*$^{-/-}$ mice from each of the four conditions were processed for sectioning. Two-to three separate airways of similar size from each lung were chosen for analysis. PAS abundance was calculated as the fraction of PAS-positive epithelium compared with the total basement membrane length. Images were visualized using an Olympus IX71 microscope with appropriate filters. For quantification of tuft cells, lung sections were stained with 4′,6-diamidino-2-phenylindole (DAPI) and anti-mouse DCLK1 antibody (cat# 62257, clone D2U3L; Cell Signaling) followed by Alexa Fluor 555 anti-rabbit-IgG secondary antibody (cat# A-11036, Invitrogen). Nine separate mouse lungs of either wild-type or *Pou2f3*$^{-/-}$ mice from each of the four conditions were processed for sectioning. Three separate airways from each lung were chosen for analysis, and the data were presented as an average for each lung. Images were visualized using a Nikon E800 microscope (Brighton, MI) with appropriate filters. Finally, additional tissue sections were stained with anti-Krt5 (cat # 905501, clone Poly19055, Biolegend) or anti-eGFP (cat # A10262, Invitrogen) antibody followed by Alexa Fluor anti-chicken-IgY (cat# A-11039; Invitrogen).

Flow cytometric analysis. Lungs were perfused with PBS containing 0.5 mM EDTA and minced and digested with Liberase TM (100 μg/ml), together with collagenase XI (250 μg/ml), hyaluronidase 1a (1 mg/ml), and DNase I (200 μg/ml; Sigma) for 1 h at room temperature. Cells were filtered and washed with RBC lysis buffer (BD Biosciences). Nonspecific binding was blocked by 1% fetal bovine serum with 1% LPS-free bovine serum albumin in DMEM, and 5 μg

rat anti-mouse CD16/32 (cat # 101302, clone 93, Biolegend) was added. To identify ILC2s, cells were stained with FITC-conjugated antibodies for lineage markers CD3ε, B220/CD45R, Ter-119, Gr-1/Ly-6G/Ly-6C, CD11b (all cat # 78022, Biolegend), CD11c (cat # 117306, clone N418, Biolegend), TCRβ (cat# 109206, clone H57-597, Biolegend), F4/80 (cat # 123108, clone BM8, Biolegend) and FcεRIα (cat # 134306, clone MAR-1, Biolegend) and anti-CD127-allophycocyanin-APC (cat # 121122, clone SB/199, eBioscience), anti-ST2-phycoerythrin(PE)-Cyanine (Cy)7 (cat # 145316, clone DIH9, Biolegend), as described (42). To identify eosinophils, cells were stained with anti-CD45-eFluor450 (cat # 48-0451-82, clone 30-F11, Invitrogen), anti-SiglecF- APC-Cy7 (cat # 565527, clone E50-2440, BD Biosciences), and anti-CD11b-APC (cat # 101212, clone M1/70, Biolegend) and negatively gated for anti-CD11c-PE-Cy7 (cat # 558079, clone HL3, BD Biosciences) and anti-Ly6G-PE (cat # 551461, clone 1A8, BD Biosciences).

Measurement of IL-25, IL-33 and TSLP protein levels. Lung IL-25, IL-33 and TSLP (Thermo Fisher Scientific) were measured by ELISA. ELISA data were analyzed by BioTek Gen5 software. Total lung protein concentration was measured by BCA protein assay (Thermo Fisher Scientific).

Measurement of airways responsiveness. Mice were anesthetized, intubated, and ventilated with a Buxco FinePointe System (Data Sciences International). Methacholine was administered methacholine via retroorbital injection (43).

Statistics. All data were represented as mean ± standard error (SE). For studies of airway responsiveness, statistical significance was assessed by two-way analysis of variance. For all other experiments, statistical significance was assessed by one-way analysis of variance. Group differences were pinpointed by the Tukey multiple comparison test. In each case, means

of each treatment group were compared with the mean of every other group, but for clarity only selected comparisons are shown.

Study approval. All animal usage was approved by the University of Michigan Institutional Animal Care and Use Committee (protocol number PRO00010065) and followed guidelines set forth in the Principles of Laboratory Animal Care from the National Society for Medical Research.

Data availability. Underlying data are available in the "Supporting data values" XLS file.

Author contributions:

YL helped design the research, performed experiments, analyzed data, interpreted results of the experiments, prepared figures, drafted the manuscript, and approved the final version of the manuscript. With MH's permission, YL was assigned first position because he reliably identified tuft cells by DCLK1 immunofluorescence and verified using ChAT-eGFP mice. MH helped design the research, performed experiments, analyzed data, interpreted results of experiments, prepared figures, drafted the manuscript, and approved the final version of the manuscript; SS performed experiments; HAB performed experiments; JEK performed experiments; CCS performed experiments; DAS performed experiments; SK performed experiments; AMG performed experiments; FK performed experiments; ATC designed research, analyzed data and prepared figures; JKB edited and revised the manuscript; IM conceived and designed the research, edited and revised the manuscript and approved the final version of the manuscript; MBH conceived and designed research, analyzed data, prepared figures, edited and revised manuscript and approved the final version of manuscript.

Acknowledgement: This work was supported NIH grants R01 AI120526 and AI155444 (to M.B. Hershenson) and R00 HL157555 (to A.T. Shenoy).

References

1. Reid L, Meyrick B, Antony VB, Chang L-Y, Crapo JD, and Reynolds HY. The mysterious pulmonary brush cell. *Am J Respir Crit Care Med.* 2005;172(1):136-9.
2. Krasteva G, Canning BJ, Hartmann P, Veres TZ, Papadakis T, Mühlfeld C, et al. Cholinergic chemosensory cells in the trachea regulate breathing. *Proc Natl Acad Sci USA* 2011;108(23):9478-83.
3. Gerbe F, Brulin B, Makrini L, Legraverend C, and Jay P. DCAMKL-1 expression identifies Tuft cells rather than stem cells in the adult mouse intestinal epithelium. *Gastroenterol.* 2009;137(6):2179-80.
4. Matsumoto I, Ohmoto M, Narukawa M, Yoshihara Y, and Abe K. Skn-1a (Pou2f3) specifies taste receptor cell lineage. *Nature Neurosci.* 2011;14(6):685-7.
5. Yamaguchi T, Yamashita J, Ohmoto M, Aoudé I, Ogura T, Luo W, et al. Skn-1a/Pou2f3 is required for the generation of Trpm5-expressing microvillous cells in the mouse main olfactory epithelium. *BMC Neurosci.* 2014;15(1):13.
6. Yamashita J, Ohmoto M, Yamaguchi T, Matsumoto I, and Hirota J. Skn-1a/Pou2f3 functions as a master regulator to generate Trpm5-expressing chemosensory cells in mice. *PLoS One.* 2017;12(12):e0189340.
7. Finger TE, Böttger B, Hansen A, Anderson KT, Alimohammadi H, and Silver WL. Solitary chemoreceptor cells in the nasal cavity serve as sentinels of respiration. *Proc Natl Acad Sci USA.* 2003;100(15):8981-6.
8. Perniss A, Liu S, Boonen B, Keshavarz M, Ruppert AL, Timm T, et al. Chemosensory cell-derived acetylcholine drives tracheal mucociliary clearance in response to virulence-associated formyl peptides. *Immunity.* 2020;52(4):683-99.e11.

9. Lee RJ, Kofonow JM, Rosen PL, Siebert AP, Chen B, Doghramji L, et al. Bitter and sweet taste receptors regulate human upper respiratory innate immunity. *J Clin Invest.* 2014;124(3):1393-405.

10. Rane CK, Jackson SR, Pastore CF, Zhao G, Weiner AI, Patel NN, et al. Development of solitary chemosensory cells in the distal lung after severe influenza injury. *Am J Physiol: Lung Cell Mol Physiol.* 2019;316(6):L1141-L9.

11. Barr J, Gentile ME, Lee S, Kotas ME, Fernanda de Mello Costa M, Holcomb NP, et al. Injury-induced pulmonary tuft cells are heterogenous, arise independent of key Type 2 cytokines, and are dispensable for dysplastic repair. *Elife.* 2022;11.

12. Huang H, Fang Y, Jiang M, Zhang Y, Biermann J, Melms JC, et al. Contribution of Trp63(CreERT2)-labeled cells to alveolar regeneration is independent of tuft cells. *Elife.* 2022;11.

13. von Moltke J, Ji M, Liang H-E, and Locksley RM. Tuft-cell-derived IL-25 regulates an intestinal ILC2–epithelial response circuit. *Nature.* 2015;529:221.

14. Gerbe F, Sidot E, Smyth DJ, Ohmoto M, Matsumoto I, Dardalhon V, et al. Intestinal epithelial tuft cells initiate type 2 mucosal immunity to helminth parasites. *Nature.* 2016;529(7585):226-30.

15. Howitt MR, Lavoie S, Michaud M, Blum AM, Tran SV, Weinstock JV, et al. Tuft cells, taste-chemosensory cells, orchestrate parasite type 2 immunity in the gut. *Science.* 2016;351(6279):1329-33.

16. Vannella KM, Ramalingam TR, Borthwick LA, Barron L, Hart KM, Thompson RW, et al. Combinatorial targeting of TSLP, IL-25, and IL-33 in type 2 cytokine–driven inflammation and fibrosis. *Science Transl Med.* 2016;8(337):337ra65.

17. Han M, Rajput C, Hong JY, Lei J, Hinde JL, Wu Q, et al. The Innate Cytokines IL-25, IL-33, and TSLP cooperate in the induction of type 2 innate lymphoid cell expansion and mucous metaplasia in rhinovirus-infected immature mice. *J Immunol.* 2017;199(4):1308-18.

18. Montoro DT, Haber AL, Biton M, Vinarsky V, Lin B, Birket SE, et al. A revised airway epithelial hierarchy includes CFTR-expressing ionocytes. *Nature.* 2018;560(7718):319-24.

19. Plasschaert LW, Žilionis R, Choo-Wing R, Savova V, Knehr J, Roma G, et al. A single-cell atlas of the airway epithelium reveals the CFTR-rich pulmonary ionocyte. *Nature.* 2018;560(7718):377-81.

20. Bankova LG, Dwyer DF, Yoshimoto E, Ualiyeva S, McGinty JW, Raff H, et al. The cysteinyl leukotriene 3 receptor regulates expansion of IL-25–producing airway brush cells leading to type 2 inflammation. *Science Immunol.* 2018;3(28):eaat9453.

21. Ualiyeva S, Hallen N, Kanaoka Y, Ledderose C, Matsumoto I, Junger WG, et al. Airway brush cells generate cysteinyl leukotrienes through the ATP sensor P2Y2. *Sci Immunol.* 2020;5(43):eaax7224.

22. Kohanski MA, Workman AD, Patel NN, Hung L-Y, Shtraks JP, Chen B, et al. Solitary chemosensory cells are a primary epithelial source of IL-25 in patients with chronic rhinosinusitis with nasal polyps. *J Allergy Clin Immunol..* 2018;142(2):460-9.e7.

23. Schneider D, Hong JY, Popova AP, Bowman ER, Linn MJ, McLean AM, et al. Neonatal rhinovirus infection induces persistent mucous metaplasia and airways hyperresponsiveness *J Immunol.* 2012;188:2894-904.

24. Hong JY, Bentley JK, Chung Y, Lei J, Steenrod JM, Chen Q, et al. Neonatal rhinovirus induces mucous metaplasia and airways hyperresponsiveness through IL-25 and type 2 innate lymphoid cells. *J Allergy Clin Immunol.* 2014;134(2):429-39.

25. Rajput C, Cui T, Han MY, Lei J, Hinde JL, Wu Q, et al. ROR alpha-dependent type 2 innate lymphoid cells are required and sufficient for mucous metaplasia in immature mice. *Am J Physiol: Lung Cell Mol Physiol.* 2017;312(6):L983-L93.

26. Rajput C, Han M, Ishikawa T, Lei J, Jazaeri S, Bentley JK, et al. Early life heterologous rhinovirus infections induce an exaggerated asthma-like phenotype. *J Allergy Clin Immunol.* 2020;146(3):571-82.e3.

27. Nadjsombati MS, McGinty JW, Lyons-Cohen MR, Jaffe JB, DiPeso L, Schneider C, et al. Detection of succinate by intestinal tuft cells triggers a type 2 innate immune circuit. *Immunity.* 2018;49(1):33-41.e7.

28. Zuo W, Zhang T, Wu DZA, Guan SP, Liew A-A, Yamamoto Y, et al. p63+Krt5+ distal airway stem cells are essential for lung regeneration. *Nature.* 2015;517(7536):616-20.

29. Lemanske Jr RF, Jackson DJ, Gangnon RE, Evans MD, Li Z, Shult PA, et al. Rhinovirus illnesses during infancy predict subsequent childhood wheezing. *J Allergy Clin Immunol.* 2005;116(3):571-7.

30. Jackson DJ, Gangnon RE, Evans MD, Roberg KA, Anderson EL, Pappas TE, et al. Wheezing rhinovirus illnesses in early life predict asthma development in high-risk children. *Am J Respir Crit Care Med.* 2008;178.

31. Rubner FJ, Jackson DJ, Evans MD, Gangnon RE, Tisler CJ, Pappas TE, et al. Early life rhinovirus wheezing, allergic sensitization, and asthma risk at adolescence. *J Allergy Clin Immunol.* 2017;139(2):501-7.

32. Kusel MM, de Klerk NH, Holt PG, Kebadze T, Johnston SL, and Sly PD. Role of respiratory viruses in acute upper and lower respiratory tract illness in the first year of life: a birth cohort study. *Pediatr Infect Dis J.* 2006;25:680-6.

33. Ualiyeva S, Lemire E, Aviles EC, Wong C, Boyd AA, Lai J, et al. Tuft cell-produced cysteinyl leukotrienes and IL-25 synergistically initiate lung type 2 inflammation. *Sci Immunol.* 2021;6(66):eabj0474.

34. Zuo W, Zhang T, Wu DZA, Guan SP, Liew A-A, Yamamoto Y, et al. p63+Krt5+ distal airway stem cells are essential for lung regeneration. *Nature.* 2014;517:616.

35. Turner RB, Hendley JO, and Gwaltney JM. Shedding of infected ciliated epithelial cells in rhinovirus colds. *J Infect Dis.* 1982;145:849-53.

36. Kang CM, Jang AS, Ahn MH, Shin JA, Kim JH, Choi YS, et al. Interleukin-25 and interleukin-13 production by alveolar macrophages in response to particles. *Am J Respir Cell Mol Biol.* 2005;33(3):290-6.

37. Wang YH, Angkasekwinai P, Lu N, Voo KS, Arima K, Hanabuchi S, et al. IL-25 augments type 2 immune responses by enhancing the expansion and functions of TSLP-DC-activated Th2 memory cells. *J Exp Med.* 2007;204(8):1837-47.

38. Roach SN, Fiege JK, Shepherd FK, Wiggen TD, Hunter RC, and Langlois RA. Respiratory influenza virus infection causes dynamic tuft cell and innate lymphoid cell changes in the small intestine. *J Virol.* 2022;96(9):e0035222.

39. Tuthill TJ, Papadopoulos NG, Jourdan P, Challinor LJ, Sharp NA, Plumpton C, et al. Mouse respiratory epithelial cells support efficient replication of human rhinovirus. *J Gen Virol.* 2003;84(Pt 10):2829-36.

40. Martin S, Casasnovas JM, Staunton DE, and Springer TA. Efficient neutralization and disruption of rhinovirus by chimeric ICAM-1/immunoglobulin molecules. *J Virol.* 1993;67(6):3561-8.

41. Newcomb DC, Sajjan U, Nanua S, Jia Y, Goldsmith AM, Bentley JK, et al. Phosphatidylinositol 3-kinase is required for rhinovirus-induced airway epithelial cell interleukin-8 expression. *J Biol Chem.* 2005;280(44):36952-61.

42. Han M, Ishikawa T, Stroupe CC, Breckenridge HA, Bentley JK, and Hershenson MB. Deficient inflammasome activation permits an exaggerated asthma phenotype in rhinovirus C-infected immature mice. *Mucosal Immunol.* 2021;14(6):1369-80.

43. Yardeni T, Eckhaus M, Morris HD, Huizing M, and Hoogstraten-Miller S. Retro-orbital injections in mice. *Lab Anim (NY).* 2011;40(5):155-60.

Figure Legends

Figure 1. RV infection induces airway tuft cell expansion. Baby mice were inoculated with sham or RV-A1B on day 6 of life and sham or RV-A2 on day 13 of life. Lungs were harvested on day 20 and processed for immunofluorescence microscopy. A) Lungs sections were stained for DCLK1 (shown in red) and DAPI (blue). Scale bars, 100 μm (insets, 50 μm). B) Group mean data for the number of cells per airway (left panel) and the fraction of airway epithelium stained positively for DCLK1 (right panel). Three airways per mouse were examined and each data point represents the average for one mouse. Data shown are mean ± SEM; n=9 mice per group from 2 different experiments; data were analyzed by one-way ANOVA. C) Immunofluorescence images show an absence of DCLK1+ cells in *Pou2f3*$^{-/-}$ mice (DCLK1, red; DAPI, blue).

Figure 2. DCLK1 and GFP colocalize in the airways of viral-infected ChAT-eGFP mice. A) ChAT-eGFP mice were inoculated with RV-A1B on day 6 of life and RV-A2 on day 13 of life. Lungs were harvested at day 20. Lungs were stained with anti-DCLK1 (red) and anti-GFP (green). There was colocalization of DCLK1 and eGFP (green). Scale bars, 100 μm. B) Lungs from RV-A1B and RV-A2-infected C57Bl/6 and *Pou2f3*$^{-/-}$ mice were harvested on day and DCLK1 and ALOX5 mRNA measured by qPCR. C) Lungs and trachea from RV-A1B and RV-A2-infected C57Bl/6 mice were stained for DCLK1 (red) and Krt5 (green). Scale bars, 100 μm. D) Lung viral copy number in C57Bl/6 and *Pou2f3*$^{-/-}$ mice. (N=6 from two different experiments, mean±SEM; data were analyzed by one-way ANOVA.

Figure 3. Pou2f3 deficiency blocks expression of innate cytokines in mice undergoing heterologous RV infection. Wild-type and *Pou2f3*$^{-/-}$ mice were inoculated with sham or RV-A1B on day 6 of life and with sham or RV-A2 on day 13 of life. Lungs from sham plus sham-, sham plus RV-A1B-, sham plus RV-A2-, and RV-A1B plus RV-A2-infected mice were harvested on day 20 for IL-25 and TSLP mRNA and ELISA and on day 14 for IL-33 mRNA and ELISA. Data shown are means ± SEM; n= 6-11 per group from 2 different experiments; data were analyzed by one-way ANOVA.

Figure 4. Pou2f3 deficiency attenuates lung ILC2 expansion in 6-day old mice following heterologous RV infection. Wild-type and *Pou2f3*$^{-/-}$ mice were inoculated with sham or RV-A1B on day 6 of life and sham or RV-A2 on day 13 of life. On day 20, lungs were harvested, digested with liberase TM, collagenase XI, hyaluronidase 1a and DNase I, and stained with Pacific blue (for dead cells), lineage antibody cocktail, anti-CD127, anti-ST2. Cells were washed, fixed, and processed for flow cytometry. A) and B) Flow cytometry analysis of live lineage-negative, CD127+ ST2+ ILC2s from sham + sham and RV-A1B + RV-A2 groups. Group mean data for ILC2s are shown (N =4-6 from two different experiments, mean±SEM; data were analyzed by one-way ANOVA.

Figure 5. Pou2f3 deficiency blocks enhanced expression of type 2 inflammation in mice undergoing heterologous RV infection. Mice were inoculated with sham or RV-A1B on day 6 of life and sham or RV-A2 on day 13 of life. A) Lungs were harvested on day 20 and processed for mRNA expression of IL-4, IL-5 and IL-13. (Data shown are mean ± SEM; n= 6 per group from 2 different experiments, data were analyzed by one-way ANOVA.) B) mRNA expression of the

pro-inflammatory cytokines IL-1β, TNF-α and IFN-γ. Lungs were harvested for qPCR on day 14 of life, one day after secondary sham or RV-A2 infection. (N=6 from two different experiments, mean±SEM; data were analyzed by one-way ANOVA.

Figure 6. Pou2f3 deficiency blocks exaggerated mucus metaplasia in mice undergoing heterologous RV infection. Mice were inoculated with sham or RV-A1B on day 6 of life and sham or RV-A2 on day 13 of life. Lungs were harvested on day 20 and processed for histology and measurement of mRNA expression. A) and B) Lung sections were stained for PAS. Large airways are shown, except for insets which show small airways. The fraction of epithelium stained positively for PAS was quantified using NIH ImageJ software. Two to three airways were examined for each mouse. Scale bars, 200 μm (insets 100 μm). C) mRNA expression of the mucus-associated genes *Muc5ac* and *Clca1*. Data shown are mean ± SEM; n=6 per group from 2 different experiments; data were analyzed by one-way ANOVA.

Figure 7. Pou2f3 deficiency blocks the asthma phenotype in viral-infected immature mice. Wild-type and *Pou2f3*$^{-/-}$ mice were infected with RV-A1B on day 6 of life and sham or RV-A2 on day 13 of life. A, B) To identify eosinophils, lung cells were stained for CD45, SiglecF and CD11b. Data shown are mean ± SEM; n=9 per group from 2 different experiments; data were analyzed by one-way ANOVA. C) Airways resistance was measured in anesthetized, intubated, and ventilated mice before and after administration of methacholine. Data shown are mean ± SEM; n=4 per group from a single experiment; data were analyzed by two-way ANOVA.

Table. Primer sequences for real-time PCR

Primers	Sequence
Mouse *Ifng* (Forward)	5’-TGGCTGTTTCTGGCTGTTAC-3’
Mouse *Ifng* (Reverse)	5’-TCCACATCTATGCCACTTGAGTT-3’
Mouse *Il1b* (Forward)	5’-TGGCAGCTACCTGTGTCTTTC-3’
Mouse *Il1b* (Reverse)	5’-GGATGGGCTCTTCTTCAAAGATG-3’
Mouse *Il5* (Forward)	5’-CTCTGTTGACAAGCAATGAGACG-3’
Mouse *Il5* (Reverse)	5’-TCTTCAGTATGTCTAGCCCCTG-3’
Mouse *Il13* (Forward)	5’-CCTGGCTCTTGCTTGCCTT-3’
Mouse *Il13* (Reverse)	5’-GGTCTTGTGTGATGTTGCTCA-3’
Mouse *Il25* (Forward)	5’-ACAGGGACTTGAATCGGGTC-3’
Mouse *Il25* (Reverse)	5’-TGGTAAAGTGGGACGGAGTTG-3’
Mouse *Il33* (Forward)	5’-GGCTGCATGCCAACGACAAGG-3’
Mouse *Il33* (Reverse)	5’-AAGGCCTGTTCCGGAGGCGA-3’
Mouse *Muc5ac* (Forward)	5’-AAAGACACCAGTAGTCACTCAGCAA-3’
Mouse *Muc5ac* (Reverse)	5’-GGTTTGACACTGACTTCCCAG-3’
Mouse *Clca1* (Forward)	5’-CTGTCTTCCTCTTGATCCTCCA-3’
Mouse *Clca1* (Reverse)	5’-CGTGGTCTATGGCGATGACG-3’
Mouse *Tnfa* (Forward)	5’-GCAGGTTCTGTCCCTTTCAG-3’
Mouse *Tnfa* (Reverse)	5’-GTCGCGGATCATGCTTTCTG-3’
Mouse *Dclk1* (Forward)	5’-TACCGACGCTATCAAGCTGGAC-3’
Mouse *Dclk1* (Reverse)	5’-GGTAACGGAACTTCTCTGGTCC-3’
Mouse *Alox5* (Forward)	5’-TCTTCCTGGCACGACTTTGCTG-3’

Mouse *Alox5* (Reverse)	5’-GCAGCCATTCAGGAACTGGTAG-3’
Mouse *Epcam* (Forward)	5’-GAGTCCGAAGAACCGACAAGGA-3’
Mouse *Epcam* (Reverse)	5’-GATGTGAACGCCTCTTGAAGCG-3’
Mouse *Tslp* (Forward)	5’-CCAGGCTACCCTGAAACTGA-3’
Mouse *Tslp* (Reverse)	5’-TCTGGAGATTGCATGAAGGA-3’
Mouse *Gapdh* (Forward)	5’-GTCGGTGTGAACGGATTTG-3’
Mouse *Gapdh* (Reverse)	5’-GTCGTTGATGGCAACAATCTC-3’

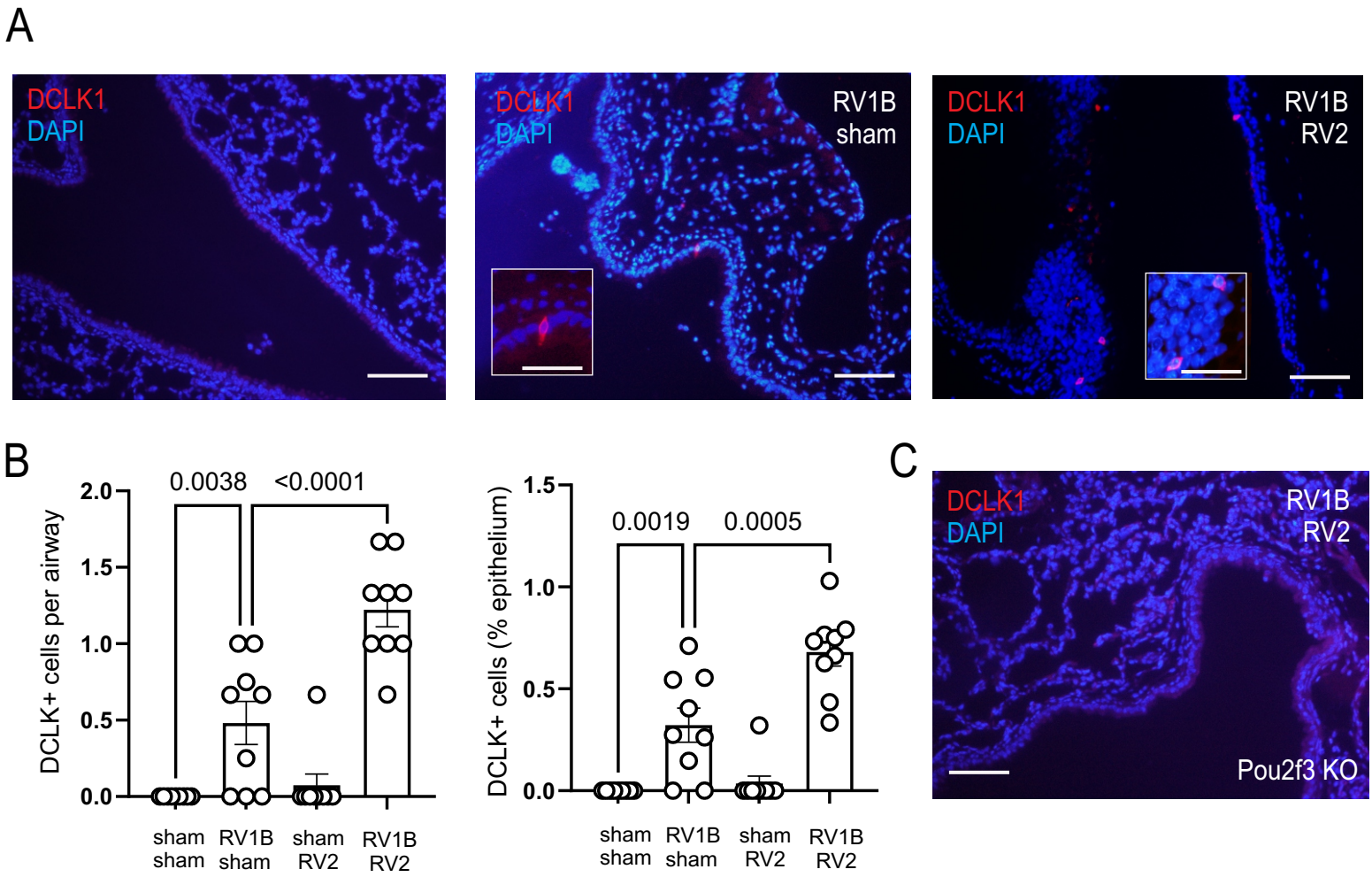

Figure 1. RV infection induces airway tuft cell expansion. Baby mice were inoculated with sham or RV-A1B on day 6 of life and sham or RV-A2 on day 13 of life. Lungs were harvested on day 20 and processed for immunofluorescence microscopy. **A)** Lungs sections were stained for DCLK1 (shown in red) and DAPI (blue). Scale bars, 100 microns (insets, 50 microns). **B)** Group mean data for the number of cells per airway (left panel) and the fraction of airway epithelium stained positively for DCLK1 (right panel). Three airways per mouse were examined and each data point represents the average for one mouse. Data shown are mean ± SEM; n=9 mice per group from 2 different experiments; data were analyzed by one-way analysis of variance. **C)** Immunofluorescence images show an absence of DCLK1+ cells in Pou2f3 KO mice (DCLK1, red; DAPI, blue).

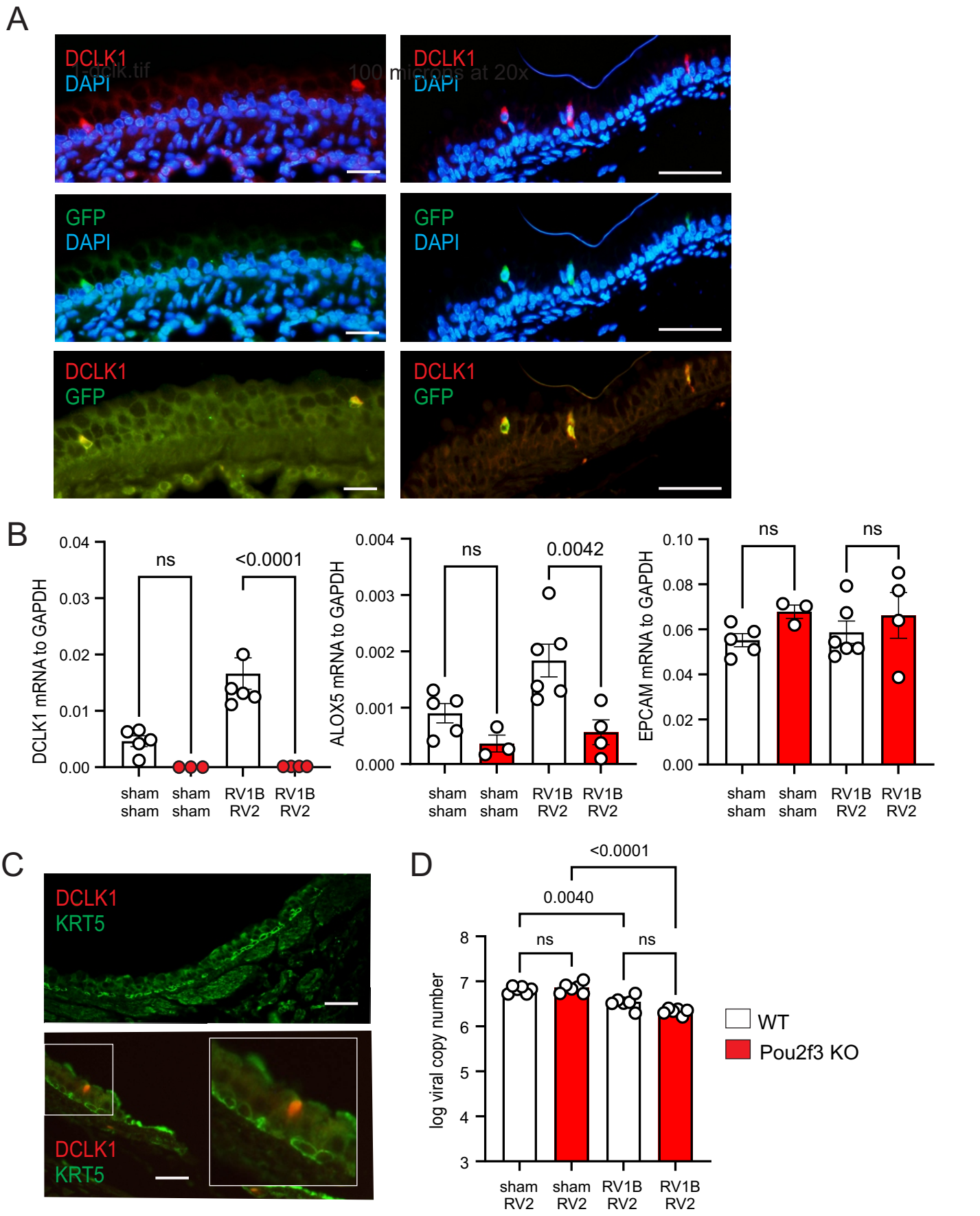

Figure 2. DCLK1 and GFP colocalize in the airways of viral-infected ChAT-eGFP mice. A) Wild type C57Bl/6 and ChAT-eGFP mice were inoculated with RV-A1B on day 6 of life and RV-A2 on day 13 of life. Lungs were harvested at day 20. Lungs were stained with anti-DCLK1 (red). There was colocalization of DCLK1 and eGFP (green). Scale bars, 100 μm. **B)** Lungs and trachea from RV-A1B and RV-A2-infected C57Bl/6 and Pou2f3 KO mice were harvested on day and DCLK1 and ALOX5 mRNA measured by qPCR. **C)** Lungs from RV-A1B and RV-A2-infected C57Bl/6 mice were stained for DCLK1 (red) and Krt5 (green). **D)** Lung viral copy number in C57Bl/6 and Pou2f3 KO mice. (N=6 from two different experiments, mean±SEM; data were analyzed by one-way ANOVA.

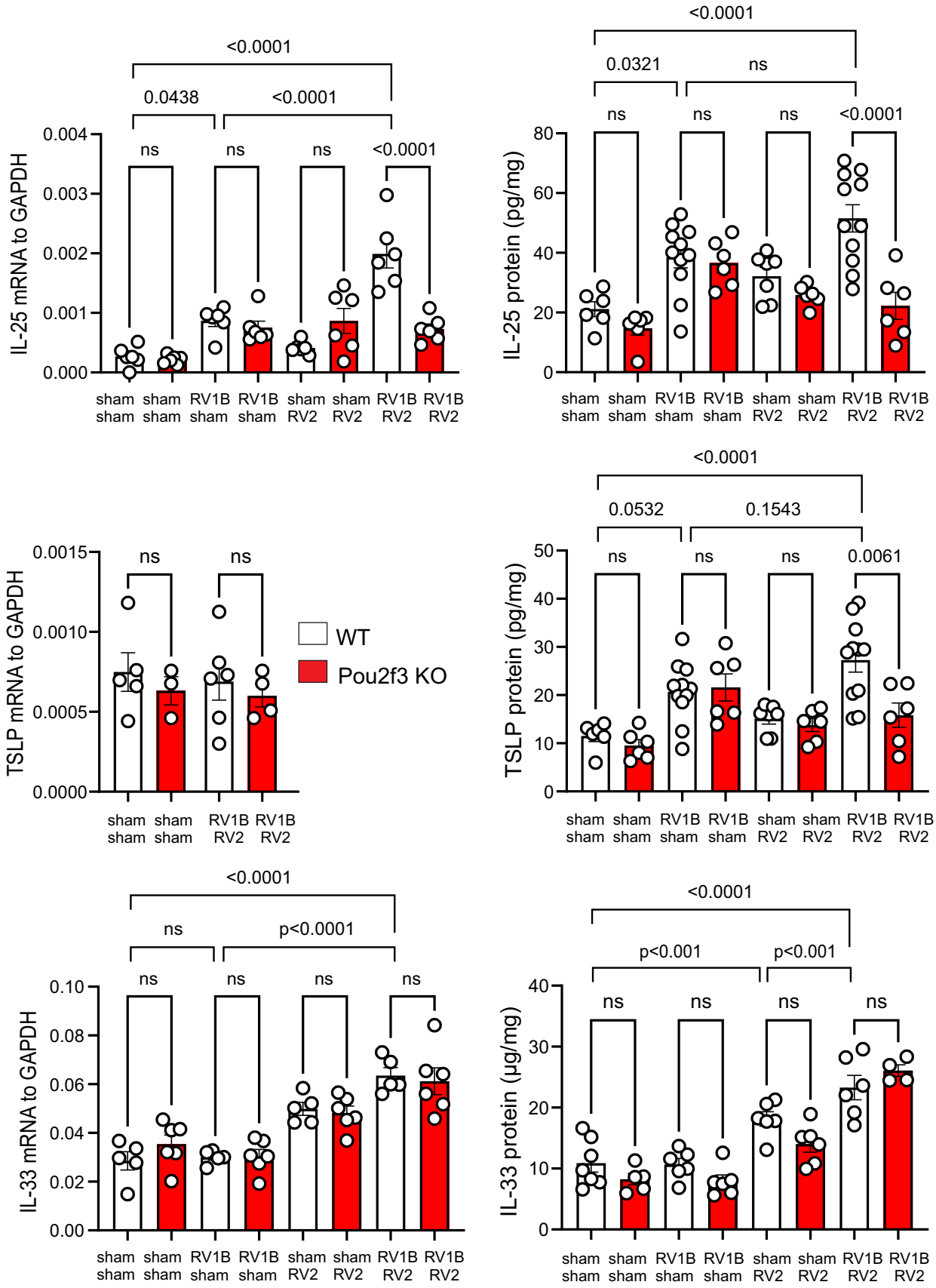

Figure 3. Pou2f3 deficiency blocks expression of innate cytokines in mice undergoing heterologous RV infection. Wild type and Skn-1a KO mice were inoculated with sham or RV-A1B on day 6 of life and with sham or RV-A2 on day 13 of life. Lungs from sham plus sham-, sham plus RV-A1B-, sham plus RV-A2-, and RV-A1B plus RV-A2-infected mice were harvested on day 20 for IL-25 and TSLP mRNA and ELISA and on day 14 for IL-33 mRNA and ELISA. Data shown are means ± SEM; n= 4-11 per group from 2 different experiments. Data were analyzed by one-way ANOVA.

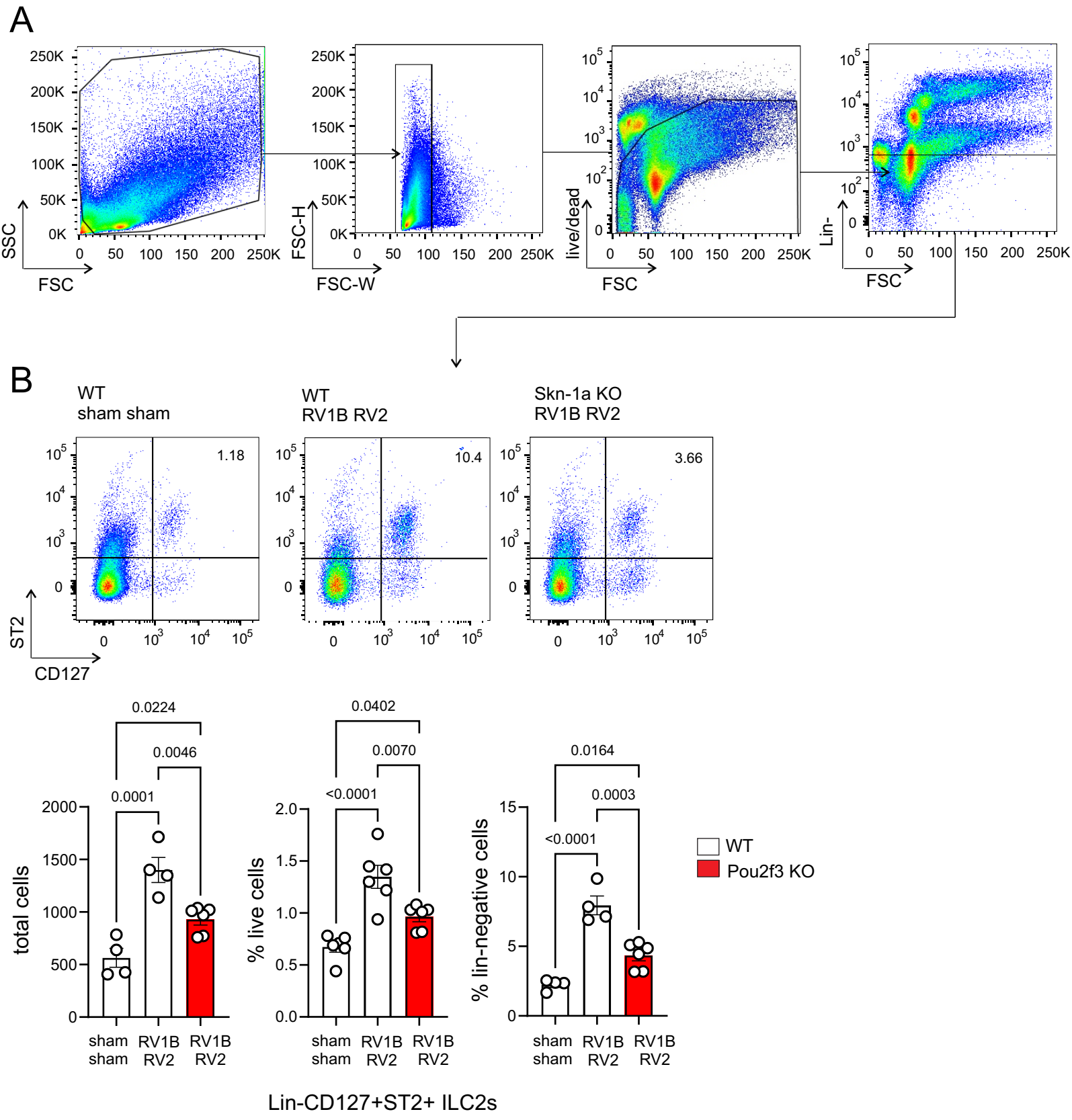

Figure 4. Pou2f3 deficiency attenuates lung ILC2 expansion in 6-day old mice following heterologous RV infection. Wild type and Pou2f3 KO mice were inoculated with sham or RV-A1B on day 6 of life and sham or RV-A2 on day 13 of life. On day 20, lungs were harvested, digested with liberase TM, collagenase XI, hyaluronidase 1a and DNase I, and stained with Pacific blue (for dead cells), lineage antibody cocktail, anti-CD127, anti-ST2. Cells were washed, fixed, and processed for flow cytometry. **A)** and **B)** Flow cytometry analysis of live lineage-negative, CD127+ ST2+ ILC2s from sham + sham and RV-A1B + RV-A2 groups. Group mean data for ILC2s are shown. (N = 6 from two different experiments, data were analyzed by one-way ANOVA.

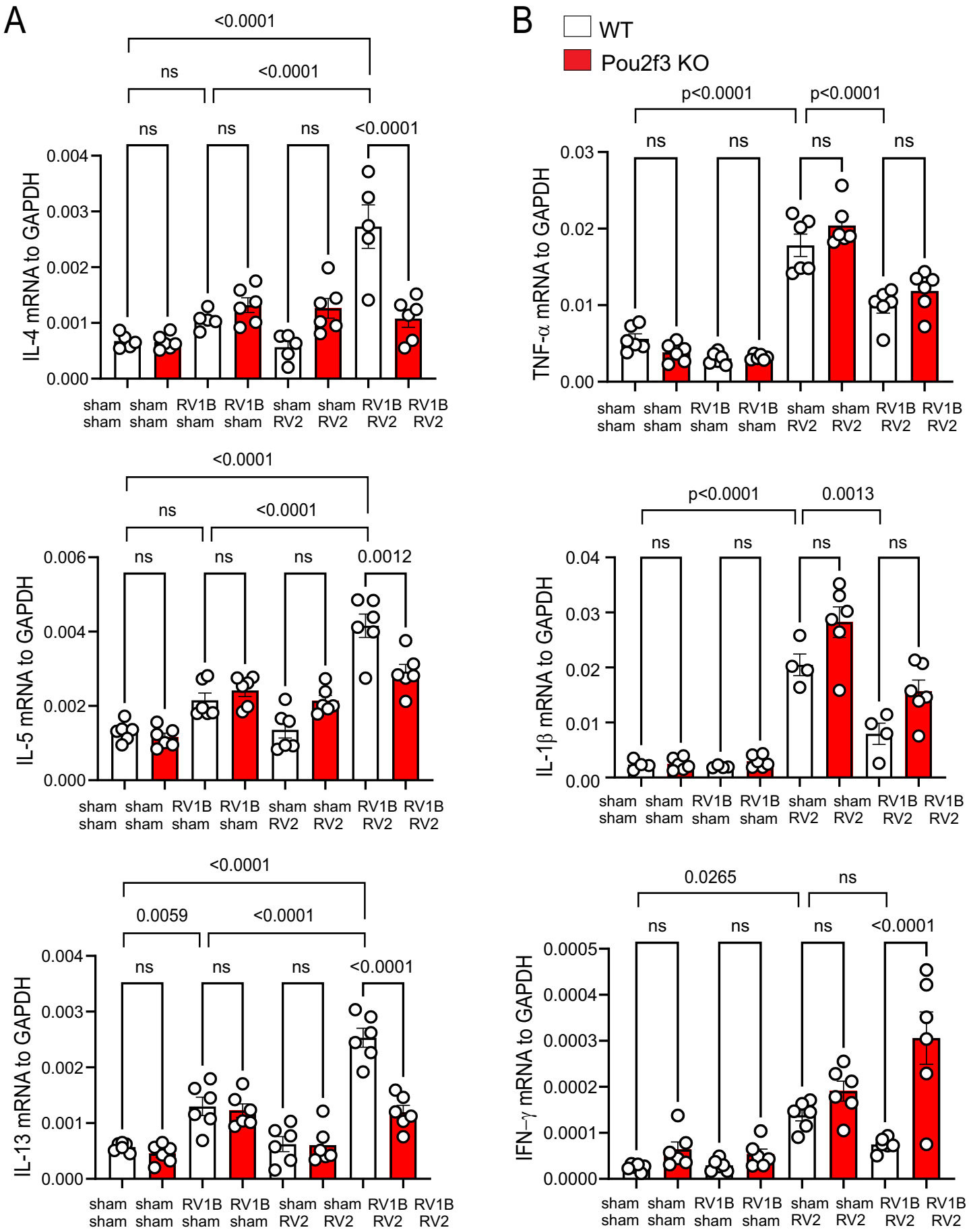

Figure 5. Pou2f3 deficiency blocks enhanced expression of type 2 inflammation in mice undergoing heterologous RV infection. Mice were inoculated with sham or RV-A1B on day 6 of life and sham or RV-A2 on day 13 of life. **A)** Lungs were harvested on day 20 and processed for mRNA expression of IL -4, IL-5 and IL-13. **B**) mRNA expression of the pro-inflammatory cytokines IL-1β, TNF-α and IFN-γ. Lungs were harvested for qPCR on day 14 of life, one day after secondary sham or RV -A2 infection. (Data shown are mean ± SEM; n= 6 per group from 2 different experiments. Data were analyzed by one -way ANOVA).

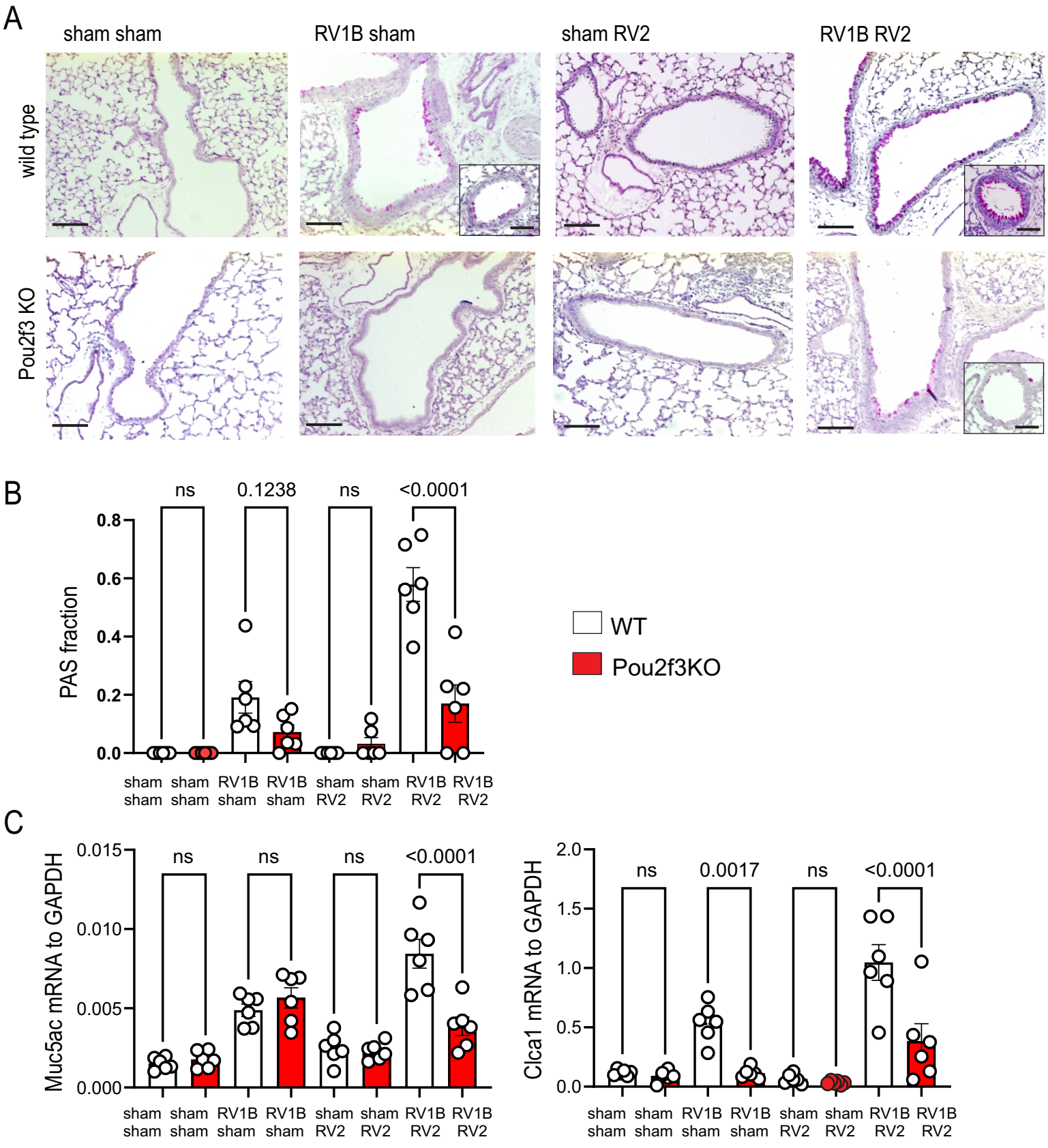

Figure 6. Pou2f3 deficiency blocks exaggerated mucus metaplasia in mice undergoing heterologous RV infection. Mice were inoculated with sham or RV-A1B on day 6 of life and sham or RV-A2 on day 13 of life. Lungs were harvested on day 20 and processed for histology and measurement of mRNA expression. **A)** and **B)** Lung sections were stained for PAS and the fraction of epithelium stained positively for PAS was quantified using NIH ImageJ software. Two to three airways were examined for each mouse. Scale bars, 200 microns (insets 100 microns). **C)** mRNA expression of the mucus-associated genes *Muc5ac* and *Clca1*. Data shown are mean ± SEM; n=6 per group from 2 different experiments; analysis by one-way ANOVA.

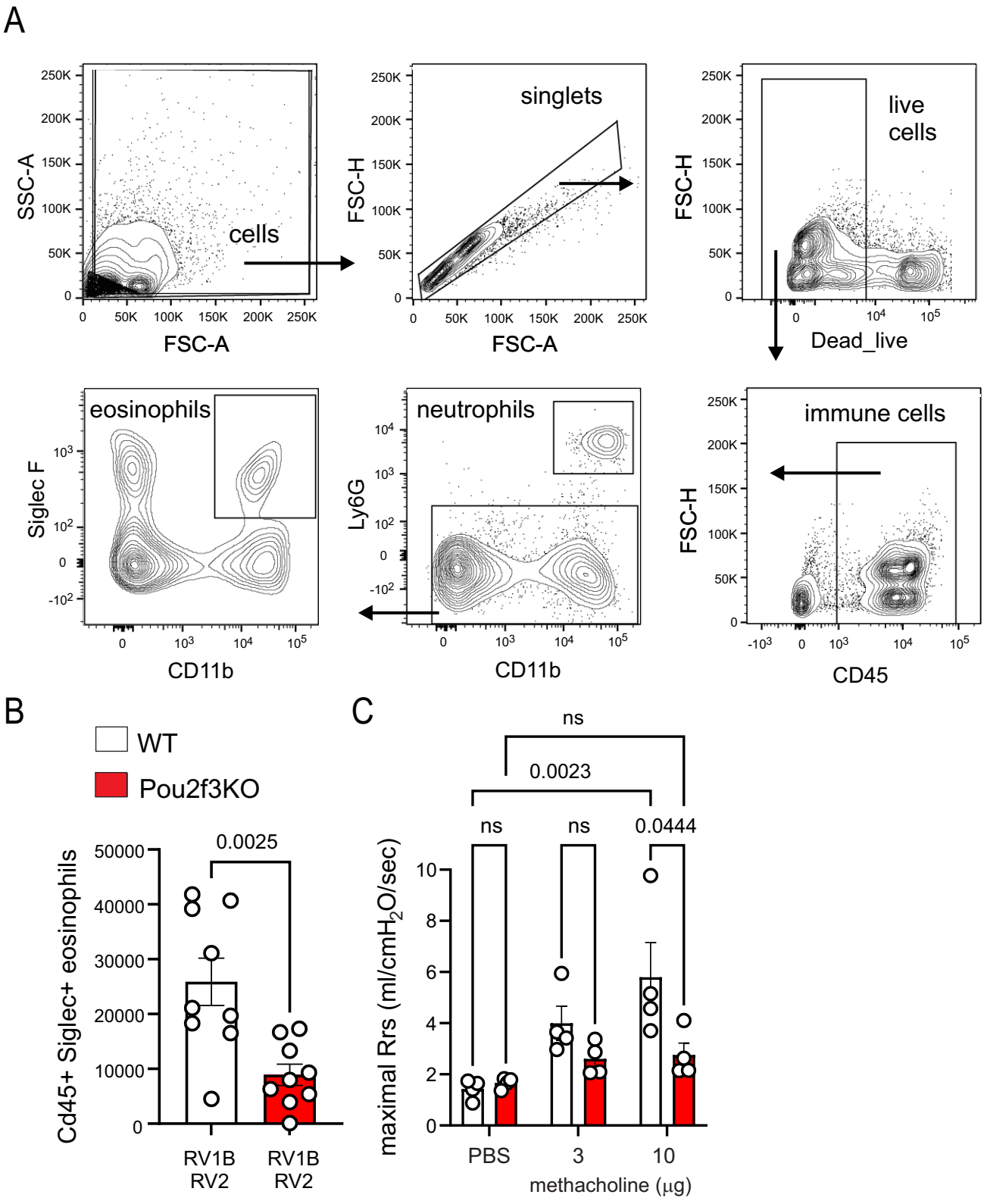

Figure 7. Pou2f3 deficiency blocks the asthma phenotype in viral -infected immature mice. C57Bl/6 and Pou2f3 mice were infected with RV -A1B on day 6 of life and sham or RV -A2 on day 13 of life. **A,B)** To identify eosinophils, lung cells were stained for CD45, SiglecF and CD11b. Data shown are mean ± SEM; n=9 per group from 2 different experiments; data were analyzed by one -way ANOVA. **C)** Airways resistance was measured in anesthetized, intubated, and ventilated mice before and after administration of methacholine. Data shown are mean ± SEM; n=4 per group from a single experiment; data were analyzed by two-way ANOVA.